Asymmetric Backward Peaking Radiation Pattern from a Relativistic Particle Accelerated by Lightning Leader Tip Electric Field

Mert Yücemöz[1] , **Martin Füllekrug**[2]

[1]University of Bath
[2]University of Bath

Key Points:

- A novel formula was developed to calculate bremsstrahlung radiation patterns of a charged non/relativistic particle with the Doppler effect.
- The bremsstrahlung radiation pattern of a charged relativistic particle exhibits forward and backward peaking due to symmetry conservation.
- The two forward and backward peaking lobes are asymmetric with respect to the velocity vector due to the curved particle trajectory.

Corresponding author: Mert Yucemoz, `m.yucemoz@bath.ac.uk`

–1–

Abstract

Terrestrial Gamma-ray Flashes exhibit slopes of ionizing radiation associated with bremsstrahlung. Bremsstrahlung has a continuous spectrum of radiation from radio waves to ionizing radiation. The Poynting vector of the emitted radiation, i.e., the radiation pattern around a single particle under the external lightning electric field during interaction with other particles or atoms, is not quite well known. The overall radiation pattern arises from the combination of radiation of parallel and perpendicular motions of a particle caused by the acceleration from the lightning electric field and the bremsstrahlung. The calculations and displays of radiation patterns are generally limited to a low-frequency approximation for radio waves and separate parallel and perpendicular motions. Here we report the radiation patterns of combined parallel and perpendicular motions from accelerated relativistic particles at low and high frequencies of the bremsstrahlung process with an external lightning electric field. The primary outcome is that radiation patterns have four relative maxima with two forward peaking and two backward peaking lobes. The asymmetry of the radiation pattern, i.e., the different intensities of forward and backward peaking lobes, are caused by the Doppler effect. A novel outcome is that bremsstrahlung has an asymmetry of the four maxima around the velocity vector caused by the curvature of the particle's trajectory as it emits radiation. This mathematical modeling helps to better understand the physical processes of a single particle's radiation pattern, which might assist the interpretation of observations with networks of radio receivers and arrays of γ-ray detectors.

1 Introduction

It was recently suggested that high-frequency radiation emissions observed in the atmosphere could originate from muons interacting with electric fields inside thunderclouds. This novel idea is based on a reduction of the muon detection during thunderstorm occurrences by the ground based telescope GRAPES-3 located in Ooty, India (Hariharan et al., 2019). Gamma-Ray Bursts (GRBs) are commonly thought to result from the interaction of neutron stars in outer space or comet collisions. GRBs emit photons in the energy range from keV to MeV that last ∼10 seconds. However, a ∼90 minute long GRB was detected with photon energies ∼18 GeV (Hurley et al., 1994). When Terrestrial Gamma-Ray Flashes (TGFs) were first observed by detectors of the Compton Gamma Ray Observatory (CGRO) (Fishman et al., 1994), their association with bremsstrahlung was demonstrated by the observation of the characteristic slopes of ionizing radiation (Dwyer et al., 2012a), supported by Monte Carlo simulations that included the bremsstrahlung process (Dwyer, 2007). Another example of bremsstrahlung associated with lightning discharges is the detection of ultra-low frequency (ULF) and very low frequency (VLF) radio emissions of the same electrons that are also responsible for emitting terrestrial gamma-ray flashes (Connaughton et al., 2013). TGFs are associated with low-frequency radio emissions, and these observations were used to identify their source altitude (Pu et al., 2019; Cummer et al., 2014). The source altitude was located to lie between two charged cloud layers in a thunderstorm. All the above discoveries offer experimental evidence for the continuous radiation spectrum of bremsstrahlung to occur. Relativistic runaway electrons are the source of high-frequency X- and γ-ray emissions observed in the upper troposphere at altitudes from ∼12-14 km height (Celestin, 2016). High energy relativistic electrons have a larger mean free path such that they can attain larger velocities until they collide with an atom or molecule in the atmosphere. As these electrons are capable of reaching large velocities, they can emit ionizing radiation through the bremsstrahlung process. Low energy electrons are much more likely to collide with atmospheric atoms or molecules, leading to an increase in the number of free electrons in the atmosphere (Celestin, 2016). Another working hypothesis is that bremsstrahlung radiation is emitted by thermal runaway electrons accelerated by intra-cloud lightning leader tips (Xu et al., 2015). Bremsstrahlung has a continuous electromagnetic spectrum. Low-frequency radio and optical emissions could also be due to fluorescence, where high-frequency TGFs

–2–

are absorbed by air molecules (Xu et al., 2015). Numerical Monte Carlo simulations demonstrated the significance of the bremsstrahlung process as the primary process behind high-frequency emissions (Dwyer et al., 2012b). Bremsstrahlung electrons emit radiation in forward peaking radiation patterns with an angle that scales with the inverse of the Lorentz factor of the relativistic electrons (Koch & Motz, 1959).

Asymmetric signal of γ-ray bursts measured by the Gamma-Ray Burst Monitor on the Fermi Gamma-ray Space Telescope reveal the lightning leader charge structure. Asymmetric γ-ray pulses indicate the lightning leader charge flux, which exhibits a fast rise and slow decay of the leader tip electric field (Foley et al., 2014). The asymmetries in γ-ray pulses are thought to be caused by Compton scattering (Xu et al., 2019). The rise to decay time ratio of single γ-ray pulses was measured to be approximately 0.67 (Nemiroff et al., 1994). Data from the Burst and Transient Source Experiment (BATSE) reveals two different types of spectra of γ-ray bursts known as bright and dim GRBs. It was found that dim GRBs have less photon energy than bright GRBs (Norris et al., 1994). It was observed that as time passes, overall γ-ray photons transit from bright to dim photons as a photon bunch due to a time delay of approximately 100 μs between the peaks arising from hard and soft photons (Grefenstette et al., 2008).
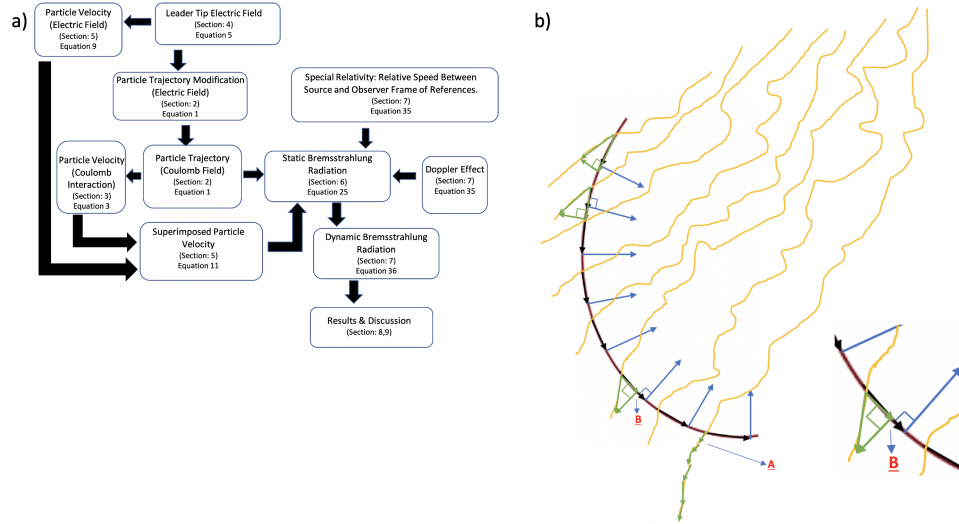
Experimental measurements of ionizing radiation and optical emissions by the Atmosphere Space Interactions Monitor (ASIM) on the International Space Station recently reported the detection of 217 TGFs from June 2, 2018, to April 1, 2019 (stgaard et al., 2019), some associated with radio emissions from charged particles that are observed on the ground. All these measurements reveal the properties of γ-ray bursts. After the combination of the measurements from ground-based radio receivers and spacecraft, it was found that TGFs are produced at the very beginning of the lightning discharge process. It is well known that the observed γ-rays originate from the bremsstrahlung process (Xu et al., 2015). There are approximately $\sim 10^{17} 10^{19}$ Gamma-ray bursts emitted during the bremsstrahlung process. It is well known that the initially emitted ionizing radiation is not the same in terms of energy and direction compared to the radiation measured by sensors. This difference is because the emitted radiation loses energy by back-scattering and interacting with other air molecules. The interaction causes an ionization and releases more electrons, which can explain why $10^{17} - 10^{19}$ γ-rays are emitted (Dwyer, 2008). Another theory explains γ-ray bursts to originate from the large electric fields of leader tip streamers producing $\sim 10^{12}$ electrons which then increase the number of electrons within the relativistic runaway electron avalanche (RREA) process that emits γ-ray photons (Babich et al., 2014, 2015a; Moss et al., 2006; Chanrion & Neubert, 2010; Celestin & Pasko, 2011; Skeltved et al., 2017).

This contribution reports the modeling of an asymmetric forward peaking radiation pattern and an asymmetric backward peaking radiation pattern of a single particle bremsstrahlung process. The asymmetry occurs around the horizontal axis parallel to the direction of motion of the charged particle, and it is unique to the bremsstrahlung process as the particle continuously follows a curved trajectory of an anticlockwise rotation. Radiation patterns are calculated for both relativistic and non-relativistic velocities. The main asymmetry with four radiation peaks is unique to the bremsstrahlung process and occurs when the particle radiation transits from a dipole towards forward and backward peaking radiation patterns.

The particle trajectory is mostly determined by the Coulomb field and modified by the presence of the external lightning leader tip electric field. The change of the particle trajectory caused by the external leader tip electric field is accounted for by only adjusting the radius of the curvature of the particle's trajectory over time. This is possible because, when the leader tip electric field is resolved into its vector components, one vector component is tangent to the trajectory, whereas, the other vector component is perpendicular to it. The perpendicular component points either in the same or opposite direction to the centripetal acceleration caused by the target particle depending on the polarity

–3–

of the leader tip electric field. The tangent component of the leader tip electric field contributes to determining the amount of angular rotation that can be covered by the particle during Coulomb interaction. The perpendicular component of the external leader tip electric field contributes to the radius of curvature of the curved trajectory caused by Coulomb interaction.

The particle trajectory defined by the Coulomb field and the particle velocity arising from the leader tip electric field are two independently derived equations that serve as ingredients that contribute to the bremsstrahlung radiation pattern (Figure 1a). This independence is important because, under a repulsive or attractive Coulomb force, the target particle mostly determines the trajectory of the incoming particle. Also, parameters defining particle trajectory by the target particles Coulomb field can account for the trajectory changes caused by the external leader tip electric field. Hence, when the radius of curvature modification caused by the external leader tip electric field is excluded from the particle trajectory, the temporal derivative of the particle trajectory is the velocity that an incoming particle experiences from the Coulomb force. The overall particle velocity is the superposition of the velocity arising from both the leader tip and the target particle's electric field. The particle velocity is considered to be dominated by the external lightning leader tip electric field.

Figure 1. a) The flow chart shows the general structure of the theory as it is developed throughout the text. b) Explains how particle's curved trajectory caused by Coulomb field changes as a result of external non-uniform leader tip electric field and how it is accounted for in the theoretical model. The yellow lines are the external electric field black arrows are the tangential Coulomb velocity, thick blue arrows are centripetal acceleration. Finally, green lines are acceleration caused by the external electric field. As can be seen in region B, one component of the leader tip electric field acceleration is in the direction of tangential Coulomb velocity. Whereas, the other component is in the opposite direction of the centripetal acceleration. Leader tip electric field acceleration in the opposite direction of the centripetal acceleration of the Coulomb field only changes the radius of curvature of the trajectory. Hence, it can be accounted with parameter "b" in the trajectory equation 1, defining the radius of curvature. The acceleration of the leader tip electric field tangent to the trajectory is accounted with the leader tip electric field velocity equation 8. Finally, region A explains how the bremsstrahlung process ends, when the leader tip electric field acceleration component opposite to centripetal acceleration is larger than the centripetal acceleration of the target particle.

1.1 Aims & Objectives

The primary aim of this contribution is to construct a generic mathematical model of electromagnetic radiation emitted by a single relativistic charged particle via the bremsstrahlung process that applies to high and low-frequency radiation. Moreover, a generic mathematical model that is also capable of explaining a particle motion whose velocity and the acceleration vectors have both parallel (particle following linear path) and perpendicular (particle following circular trajectory) orientations with each other, at the same time. The secondary aim is to use the model to investigate the details of the actual particle motion and radiation mechanisms during the bremsstrahlung process. Initial assumptions for the particle position vector and lightning leader tip electric field were made to achieve the stated aims. In addition, all the necessary physical details of the interaction, such as form factors and collision cross-sections, are included and investigated. They both play a crucial role in explaining high-frequency radiation. Moreover, the Doppler effect was added to transform the model from a static to a dynamic model. Transformation enables an explanation of the asymmetry of the radiation in forward and backward direction relative to the axis perpendicular to the particle's direction of motion. Finally, the second-order differential equation (Eq. 13) was solved as an initial step to establish a generic model to explain radiation patterns using algebra, calculus, geometry, and the table of integral transforms.
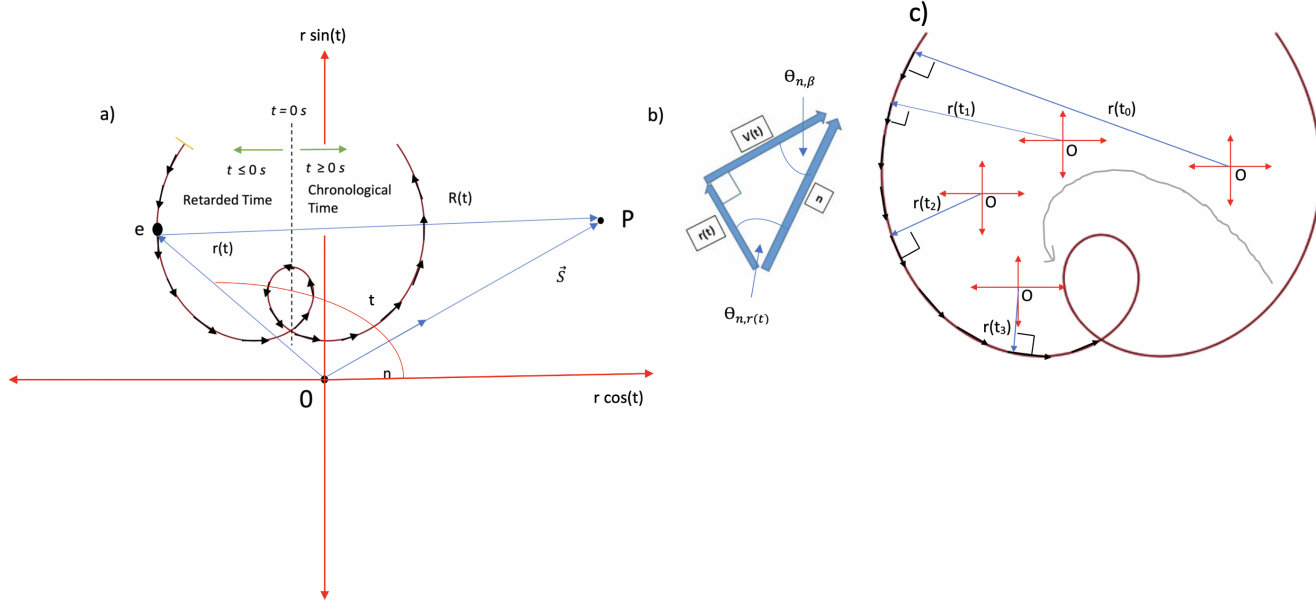
2 Particle Position Vector

Starting with defining a curved path for a bremsstrahlung electron.

The position vector is formulated for a particle trajectory that is an anti-clockwise rotating spiral as a function of the retarded time characteristic for bremsstrahlung radiation.

The position vector in equation 1 defines a spiral trajectory for an incoming particle, i.e., an electron, induced by the Coulomb force of the target particle that causes the emission of bremsstrahlung radiation (Figure 2a). The spiral trajectory in Figure 2a and mathematically defined in equation 1 is realistic even though the mean free path is quite short, e.g., nm-μm in the atmosphere with a high recombination rate. For example, a circle with a radius of 1 m could also have a radius of 2 μm, depending on the medium and the recombination rate. It is still a circle but a scaled microscopic version of the initial macroscopic circle. Preserving geometry at different scales is also true in the formulated spiral trajectory (Eq.1). The decision on a specific particle trajectory considers the ratio of particle size to a curved trajectory radius. If the particle size is larger than the curvature radius, the particle trajectory is approximately a straight line. Therefore, a spiral particle trajectory is realistic because an electron has a size of $< 2.8 \times 10^{-19}$ m as measured by the Hadron-Electron Ring Accelerator (HERA) in Hamburg, Germany at the Deutsches Electronen Synchrotron (DESY) facility (Bourilkov, 2000).

Overall acceleration caused by the Coulomb field can be resolved into its orthogonal components as centripetal and tangent Coulomb accelerations. The centripetal acceleration caused by the target particle defines the curved trajectory of the incoming particle and it is this centripetal acceleration that forces the incoming particle to stay on its curved trajectory. The tangent Coulomb velocity and acceleration components caused by the target particle due to the Coulomb field are perpendicular to the position and centripetal acceleration vectors. Hence, tangent to the particles curved trajectory.

Similar to Coulomb field, leader tip electric field can also be resolved into its orthogonal vector components. As shown in figure 1b, tangent to the particle trajectory component of the leader tip electric field increases the incoming particle's tangential Coulomb velocity, hence acceleration. The remaining acceleration component of the external lightning electric field acts in the opposite direction to centripetal acceleration and it only changes the radius of curvature of the incoming particles trajectory which can be accounted with mathematical variable b in equation 1 representing particles radius of curvature.

Figure 2. a) Trajectory of the bremsstrahlung electrons given by equation (1) in a polar co-ordinate system and radiation emissions by the change in velocity over time by a Coulomb force of other charges. O represents the target particle that defines the electron's spiral trajectory due to the Coulomb force (equation 1). The tangential component of the electron acceleration and corresponding velocity vectors are displayed with black arrows and are tangential to the spiral trajectory (red line) and perpendicular to the position vector $r(t)$. $R(t_r)$ is the distance between the accelerated electron and the observer, which is a function of both retarded and chronological time (t_r, t). P is the position of an observer. $\vec{S}$ is the Poynting vector, or radiant energy flux, which determines the direction of the energy flow per area of an emitted electromagnetic wave. The dimensionless unit vector n points in the direction of the Poynting vector $\vec{S}$. b) The position vector $r(t)$, velocity vector $v(t)$ and the unit radiation vector n form a rectangular triangle. c) Co-ordinate system and all the associated vectors are drawn from the target particle which is positioned at the origin, O. As the target particle is not a rigid body and displaces under the incoming particle's Coulomb field, the moving co-ordinate system is constructed (Brock, 2019). Displacement of the moving co-ordinate system is described with the collision cross-section and form factors (Supplemental information, text S2). Position vector, r(t) connects both target and incoming particle together. Time derivative of this position vector is the tangential velocity of the incoming particle and it is perpendicular to the position vector in the moving co-ordinate system. Without radius of trajectory changes caused by the external leader tip electric field, time derivative of the position vector is the tangential component of the Coulomb velocity. With radius of trajectory changes caused by the external leader tip electric field, time derivative of the position vector is the tangential component of the overall velocity.

$$r(t) = \frac{(t^R)^2 b^R (\omega')^R \cos(\theta_{n,r(t)})^R c}{\tau^{2R} c^R \omega' \cos(\theta_{n,r(t)})} - \frac{at}{\tau}, \tag{1}$$

where $r(t)$ is the position vector as a function of time t in s, R is the dimensionless bremsstrahlung asymmetry index, τ is the mean free time in s. Also, ω' is the angular frequency of the emitted electromagnetic wave in the frame of reference of the particle in rads/s, c is the speed of light, $\theta_{n,r(t)}$ is the angle between

186 the emitted radiation unit vector n and the particle's position vector. The time range of the position vector
187 is $-\infty < t < +\infty$. In addition, the factor b in m describes the interaction distance between the incoming
188 particle and the target particle, which is the radius of the time-dependent position vector. The radius of the
189 position vector is directly proportional to the parameter b. This radius of curvature is related to the mean
190 free path because the curvature increases with time, contributing to the overall arc length, i.e., the mean free
191 path of the accelerated particle. In other words, $b \propto \lambda_{v/c}$, where $\lambda_{v/c}$ is the mean free path of a particle at the
192 velocity v which is given as a percentage of the speed of light v/c. The relation between a and $\lambda_{v/c}$ will be
193 derived in section 3. The factor a in m is an arbitrary adjustment parameter. It is introduced to correct the
194 radius of the curvature of a particle during the bremsstrahlung process. This correction is required because
195 the trajectory of a relativistic particle shrinks in size over time, and a propagation close to the speed of light
196 introduces significant changes in the mean free path. Finally, equation 1 is a function of time t. Hence, the
197 particle will only cover some segment, or arc length, of the spiral, or the complete arc length of a particle's
198 spiral trajectory when $t = \tau$.

3 Interaction Gap

200 Defining the mean free path, $\lambda_{v/c}$ and the particle velocity arising only from the
201 Coulomb interaction, $\frac{dr}{dt}$.

The arc length, or the mean free path, of a curve in polar coordinates is given by

$$\lambda_{v/c} = \int_0^{\theta_f} \sqrt{r^2 + \left(\frac{dr}{d\theta}\right)^2}\, d\theta, \tag{2}$$

202 where $\lambda_{v/c}$ is the mean free path, r is the position vector given in equation 1, and the
203 derivative with respect to the polar angle is $\frac{dr}{d\theta}$. Equation (2) is a geometric equation used
204 to calculate the arc length of any curve in polar coordinates. As the particle covers its
205 mean free path, it follows the curved spiral trajectory in small segments with time t. In
206 this case, equation (2) has to be formulated with the parameter t rather than θ. To sat-
207 isfy the dimensional accuracy, the Jacobian is used to carry out a variable transform from
208 θ to t to preserve the dimension m^2 in the square root of the integrand. In geometry, the
209 unit of angle in rad is considered to be dimensionless. An example of this is the arc length
210 formula of a circle ($s = r\theta$). Hence, $\theta = \frac{t}{\tau}$. The mean free time τ is a function of time
211 due to its dependence on particle velocity that changes over time. Therefore, the quo-
212 tient rule $\left(\frac{d\theta}{dt} = \frac{\Lambda\frac{du}{dt} - u\frac{d\Lambda}{dt}}{\Lambda^2}\right)$ has to be used to find the derivative $\frac{d\theta}{dt}$. Input parame-
213 ters to the quotient rule are, $u = t$, $\Lambda = \tau$, $\frac{du}{dt} = 1$ and $\frac{d\Lambda}{dt} = \tau'$ where τ' is the first
214 derivative of the mean free time with respect to time t. The mean free time τ of the two
215 identical particles is defined as $\tau = \frac{1}{\pi n v d^2}$, where n is the particle or molecule number
216 density per unit volume in m^{-3} and d is the diameter in m of both an incoming and a
217 target particle or molecule. The basic mean free time is defined between two identical
218 particles with same diameter d where effective collision area is defined as a function of
219 the two identical particle's diameter as $A_c = \pi d^2$. Finally, $\frac{d\theta}{dt} = \frac{\tau - t\tau'}{\tau^2}$ and the limits
220 of the integration are $0 \le \frac{t}{\tau} \le \theta_f = 1$ rad. The maximum limit of the integral is 1,
221 which means that the ratio of t to τ as time progresses should not exceed allowed mean
222 free time τ for the particle to radiate.

223 Coulomb velocity of an incoming particle arising from electrostatic interaction be-
224 tween a target particle can be written as

$$\frac{dr}{dt} = \frac{b^R(\omega')^R cos(\theta_{n,r(t)})^R c}{c^R \omega' cos(\theta_{n,r(t)})} \left(\frac{\tau^{2R}\left[t^{2R}\frac{2R}{t} + t^{2R}2R'ln(t)\right] - t^{2R}\left[\tau^{2R}\frac{2R}{\tau} + \tau^{2R}2R'ln(\tau)\right]}{\tau^{4R}}\right) - \frac{a\tau - at\tau'}{\tau^2}. \tag{3}$$

–7–

225 Second terms, $t^{2R}2R'ln(t)$ and $\tau^{2R}2R'ln(\tau)$ inside the square brackets of the equation 3 represents a
226 trajectory of varying radius of curvature i.e. spiral. Changing radius of curvature with time is directly
227 linked to the changing bremsstrahlung asymmetry, R with time, R'. In the case of $R' = 0$, particle
228 follows a constant radius trajectory where the bremsstrahlung asymmetry, R remains at a constant value.
229 Such trajectory could be a circle.

230 This leads to

$$\lambda_{v/c} = \int_0^1 \sqrt{r^2 + \left(\frac{dr}{dt}\frac{\tau^2}{(\tau - t\tau')}\right)^2} \frac{\tau - t\tau'}{\tau^2} dt. \qquad (4)$$

231 Equation 4 means that by knowing the mean free path of an electron in the atmosphere, the parameters
232 a and b of a position vector $r(t)$ in equation one can be calculated.

4 Lightning Leader Tip Electric Field

234 In this section, the lightning leader tip electric field is formulated to define the particle velocity for
235 the bremsstrahlung radiation. The velocity defined by an integration of the electric field can be equated to the
236 formulated velocity (equation 3) from the particle position vector to calculate the unknown parameters a and b.
237 Moreover, this is an important step in defining particle velocity parameters such as the mean free path and time
238 as the leader tip electric fields can be measured experimentally.

239 The measured lightning discharge electric field has a characteristic behavior of a sharp rise and
240 a slow decay. This characteristic information was used to mathematically model the lightning leader tip
241 electric field, E in equation 5. The electric field is mathematically modeled using the ansatz of a sharp rise
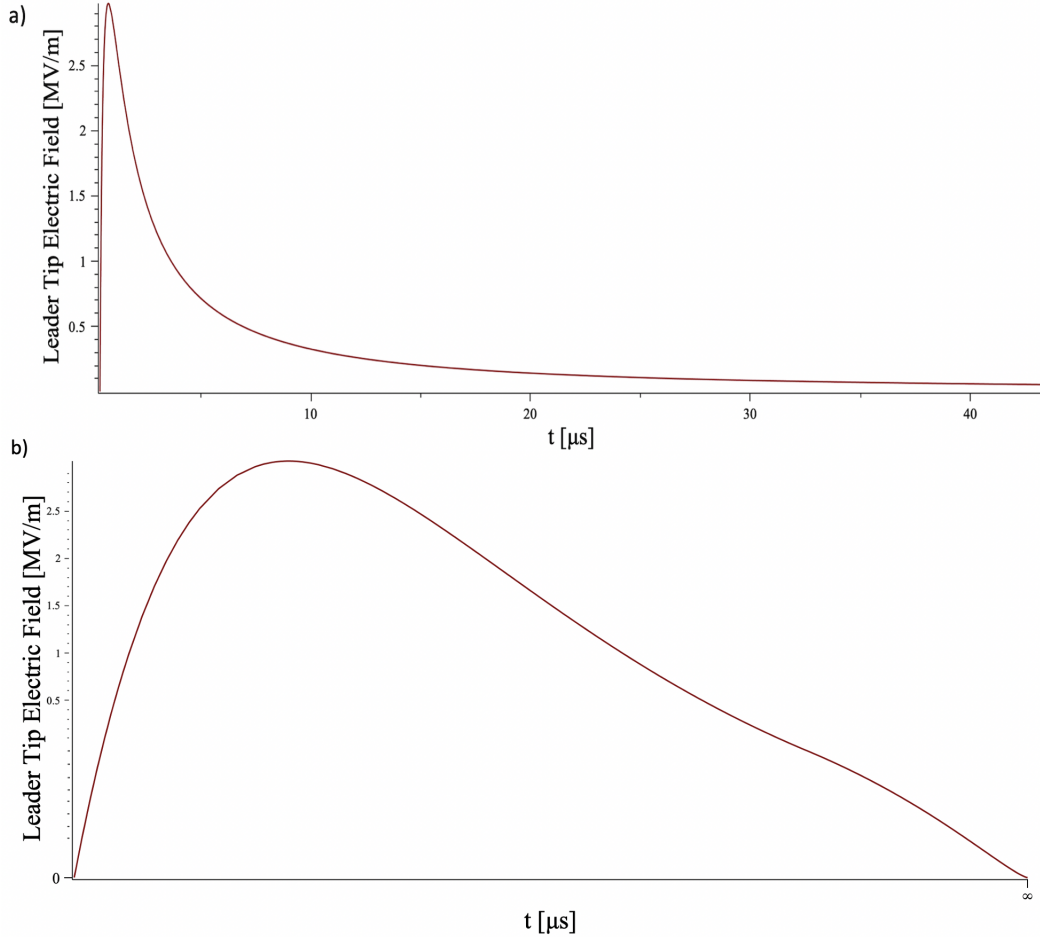242 and a slow decay

$$E(t) = s_f \left[\frac{An(s_{ft})^{(n-0.489)}}{(t/t_0)^{(n-0.489)}} - \frac{2B(s_{ft})^m}{(t/t_0)^m} \right], \qquad (5)$$

243 where $A = 4.083 \times 10^7$ $[\frac{J}{Cm}]$ or $\frac{V}{m}$, $B = 3.840 \times 10^7$ $[\frac{J}{Cm}]$ or $[\frac{V}{m}]$, $n = 1.95$ is a dimensionless
244 constant, and $m = 1.5$ is a dimensionless constant. The scaling factor $s_f = 1$ scales the lightning
245 leader tip electric field magnitude, i.e., it is a dimensionless constant that can be used with different
246 constant values to adjust the leader tip electric field to the required strength, $s_{ft} = 1$ is a dimensionless
247 constant scaling factor of time, and the time t/t_0 is the relative time with respect to $t_0 = 1$ s where $t[s]$ is
248 an independent time variable. The time range of the electric field is $s_{ft}\, 0.39694$ μs $\le t \le \infty$.
249 Values closer to 0.397 μs describe the initial state and values closer to 72.2 μs describe the final state
250 of the lightning leader tip electric field shown in Figure 3. The minimum value of time was determined such
251 that it is the minimum value of the electric field before it goes to $-\infty$ at $t = 0$ s. The scaling factor determines
252 the acceleration of the particle. As a result, the magnitude of the emitted radiation intensity scales in an
253 indirect way by scaling the electric field which scales the force and hence the acceleration.

254 The lightning leader tip electric field in equation (5) is derived such that it goes to zero at infinite time,
255 as shown in Figure 3b. Any remaining residual electric field integrated over infinite time would accelerate
256 a particle to velocities exceeding the speed of light.

257 The strength and duration of the electric field affect the magnitude and pattern
258 of the emitted radiation. To adjust the electric field's strength and duration conveniently
259 without affecting the graphical shape of Figure 3a, the scaling factor s_f for magnitude
260 and s_{ft} for the duration are introduced.

Figure 3. Derived electric field in equation 5. a) The leader tip electric field is modeled to fit observed electric field characteristics of lightning discharges. Lightning discharges exhibit a sharp rise and slowly decaying electric field. The peak value of the electric field was chosen to be ~ 3 MV/m, which is the approximate electric field for the conventional dielectric breakdown of air. For a RREA to develop, the electrons need to be relativistic such that bremsstrahlung occurs. In this case, the leader tip electric eld is on the order of ~ 26 MV/m at 101 kPa of atmospheric pressure (Babich et al., 2015b). b) The derived electric field from $0\ s$ to ∞ is plotted on logarithmic time scale. It is important that the leader tip electric field is 0 V/m at infinity. Any function used to describe the leader tip electric field that never goes to zero (i.e., an exponential) integrated up to infinity would cause a particle to exceed the speed of light.

5 Velocity Function

The velocity of the particle accelerated by the leader tip electric field is found by integrating the derived electric field (Figure 3, Eq. 5). The upper and lower limits of the integration are chosen such that the result of the integral gives a velocity equation as a function of time. Next, the solution of integral is scaled to accelerate the particle up to 94% of the speed of light, i.e., 280,000 km/s, and thereby prevents the particle from exceeding the speed of light in vacuum, c. Finally, the particle velocity function should decay to the thermal velocity. Afterward, the particle should either remain constant at a thermal velocity or slowly decay to 0 m/s and remain stationary at an infinite time for the particle to stop radiating. A stationary or constant velocity at infinite time is im-

–9–

271 portant because equation 13 requires an integral with limits between $\mp\infty$, and the par-
272 ticle cannot radiate for an infinite time. The derived velocity function (Eq. 9) presented
273 in Figure 4 accelerates the particle from a thermal velocity (92.493 km/s) up to 94% of
274 c within $\sim$ 12.427 ns and then decelerates back to a thermal velocity. The whole pro-
275 cess takes $\sim$ 24.854 ns.

276 The velocity function is the integral of the electric field function with respect to
277 time, multiplied with the constant charged particle properties, which are elementary charge
278 e, charge number z, and the inverse of accelerated electron mass $\frac{1}{m_e}$.

$$v(t) = \frac{ez}{m_e} \int_{s_{ft}0.39694\mu s + \left|\frac{t[s]}{t_o[s]}\right||t_o}^{\infty} E(t)dt. \tag{6}$$

279 Where $t_o = 1$ s . The upper limit was set to be infinite in order to prevent the
280 lower boundary of the integral from exceeding the upper limit. The lower limit involves
281 a time parameter to prevent the indefinite integral from being a definite integral in or-
282 der to create a velocity function. The absolute time is used here to create a symmetric
283 velocity behavior in retarded time to explain the particle motion and also to satisfy the
284 integral limits between $\mp\infty$ in equation 13. The factorial was incorporated in order to
285 prevent the electric field from becoming singular at $t = 0$ s.

286 Separating integral (Eq. 6) into the two terms of the electric field function (Eq. 5)
287 gives

$$v(t) = \frac{ez}{m_e}s_f A n s_{ft}^{(n-1.489+1)} \int_{s_{ft}0.39694\mu s+|t|!}^{\infty} \frac{1}{(t)^{(n-1.489)}t}dt - \frac{ez}{m_e}s_f 2B s_{ft}^m \int_{s_{ft}0.39694\mu s+|t|!}^{\infty} \frac{1}{t^m}dt \tag{7}$$

and

$$v(t) = \frac{ez}{m_e}s_f A n (s_{ft})^{(n-1.489+1)}$$
$$\left[\frac{(125)2^{2.511+n}3^{n-0.489}(9.657\times10^6)^{n-0.489}(23s_{ft}+5.794\times10^7|t|!)^{-n+0.489}(3.969\times10^7 s_{ft}+|t|!)}{1000n-1489}\right]$$
$$-\frac{ez}{m_e}s_f 2B(s_{ft})^m\left[\frac{(3.969\times10^{-7}s_{ft}+|t|!)^{-m+1}}{-1+m}\right]. \tag{8}$$

288 The factorial of time only works for an integer number of time values. However,
289 this is only a problem when the velocity function is used with non-integer values. To ap-
290 proximate velocities with a factorial of non-integer time values, Stirling's approximation
291 can be used. The velocity function can be written with the substitution of all the con-
292 stant values that do not require to be changed in order to scale. Also, to preserve the
293 physical meaning of the characteristic lightning leader tip electric field feature with a sharp
294 rise and a slow decay taking place in the atmosphere. These constants are A, B, n, and
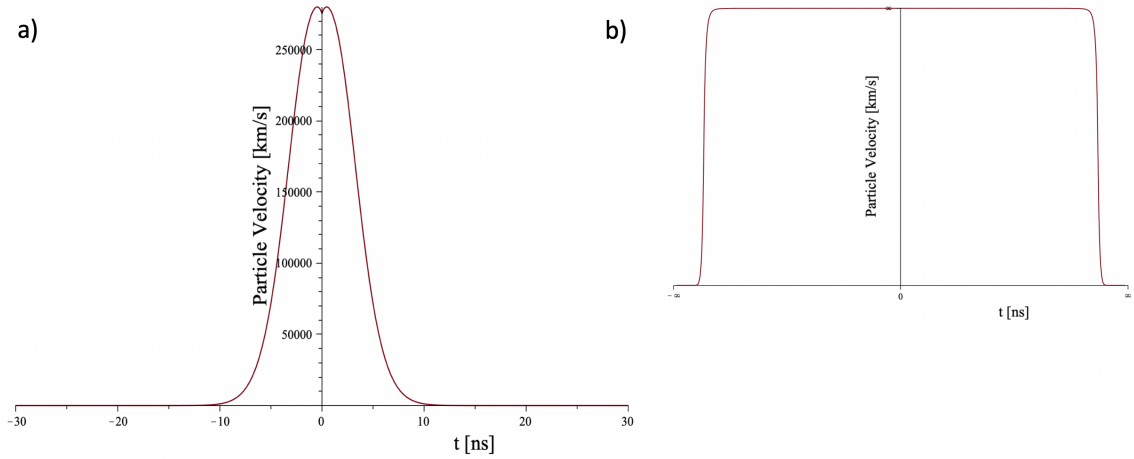295 m. Substituting and simplifying gives

$$v(t) = s_{fv}s_f z(s_{ft})^{1.461}\frac{4.365\times10^{26}}{(1.333\times10^9 s_{ft}+3.357\times10^{15}|s_{ftv}t|!)^{0.461}}-$$
$$s_{fv}s_f z(s_{ft})^{1.5}\frac{1.565\times10^{27}}{((1.333\times10^9 s_{ft}+3.357\times10^{15}|s_{ftv}t|!)^{0.5}}. \tag{9}$$

296 As the particle has a short mean free path with a short mean free time $\sim$ns, the time scale in the velocity
297 function (8) was scaled accordingly to ns with $s_{ftv} = 1\times10^9$ to reflect atmospheric electrodynamic conditions.

–10–

298 Previous to the scaling, as the time t is integrated up to ∞, the time scaling in the velocity function (8) has
299 grown and it took ~ 12.427 s for the electron to reach 94% of the speed of light from its thermal velocity
300 $v_{rms} = \sqrt{\frac{3kT}{m}}$ of 92.493 km/s at an example ambient air temperature of 188.15 K, when considering the
301 mesosphere at an altitude of 80 km. Similarly, as the time t is integrated up to ∞, the particle attained a
302 large velocity with the multiplication of the constant term $\frac{ez}{m_e}$ in front of the integral. This is solved with a new
303 velocity scaling factor $s_{fv} = 8.19 \times 10^{-11}$.

304 By knowing the particle velocity, the particle velocity equation (Eq. 9) can be scaled directly by using
305 the corresponding scaling factors for the required velocity. The mean free path (Eq. 4) of a particle is a
306 function of the total particle velocity. Although the derivative of the position vector (Eq. 3) alone determines the
307 velocity arising from the Coulomb force, equation 3 is the total velocity when used for the mean free path
308 (Eq. 4). Hence, if the particle velocity is known, it can be equated to the derivative of the position vector on
309 a spiral trajectory (Eq. 3) to determine the parameters a (the relativistic mean free path correction parameter)
310 and b (the interaction distance between an incoming and a target particle). This algebraic calculation transforms
311 the velocity arising from the Coulomb field, i.e., the derivative of the position vector in equation 1, to an overall
312 velocity, i.e., the sum of the velocity arising from the Coulomb field and the velocity originating from the
313 external lighting leader tip electric field for a particle on a spiral trajectory.

314 As can be seen from Figure 4, the above assumptions help to construct a velocity function (Eq. 9). The
315 complete radiation model is based on the fact that the particle reaches approximately 94% of the speed of light.
316 Then the particle decelerates back to a thermal velocity as bremsstrahlung is the braking radiation due to
317 obstacle particles or atoms, and as the source electric field from the leader tip starts to decay.

Figure 4. Velocity function (Eq. 9) of the derived electric field. (a) There is no negative
chronological time. However, negative time has a meaning in physics that it describes an off the
record process of an experimentally observed electromagnetic pulse. Negative time is the retarded
time in LinardWiechert potentials that describes the radiation emission by the acceleration of a
single particle. Retarded time in LinardWiechert potentials is also the reason why equation (13)
has integral limits between $-\infty$ and ∞. Negative time describes the duration of the process until
the pulse detection time of the observer. Therefore, starting from $\sim$-10 ns up to to $\sim$10 ns, the
particle gains velocity through an acceleration by the external leader tip electric field, and as it
accelerates, it radiates electromagnetic radiation. When the particle velocity is peaking around
$t = 0$ s, the observer starts receiving a signal and can measure the pulse as the process of particle
acceleration, and the propagation of the electromagnetic wave from the source to an observer
requires some time - known as the retarded, or negative, time. b) The electron's velocity on an
infinite time scale displays the end of a particle acceleration outside the range of $\sim \mp 11$ ns until
$\mp\infty$. The peak velocity remains the same at 94% of the speed of light.
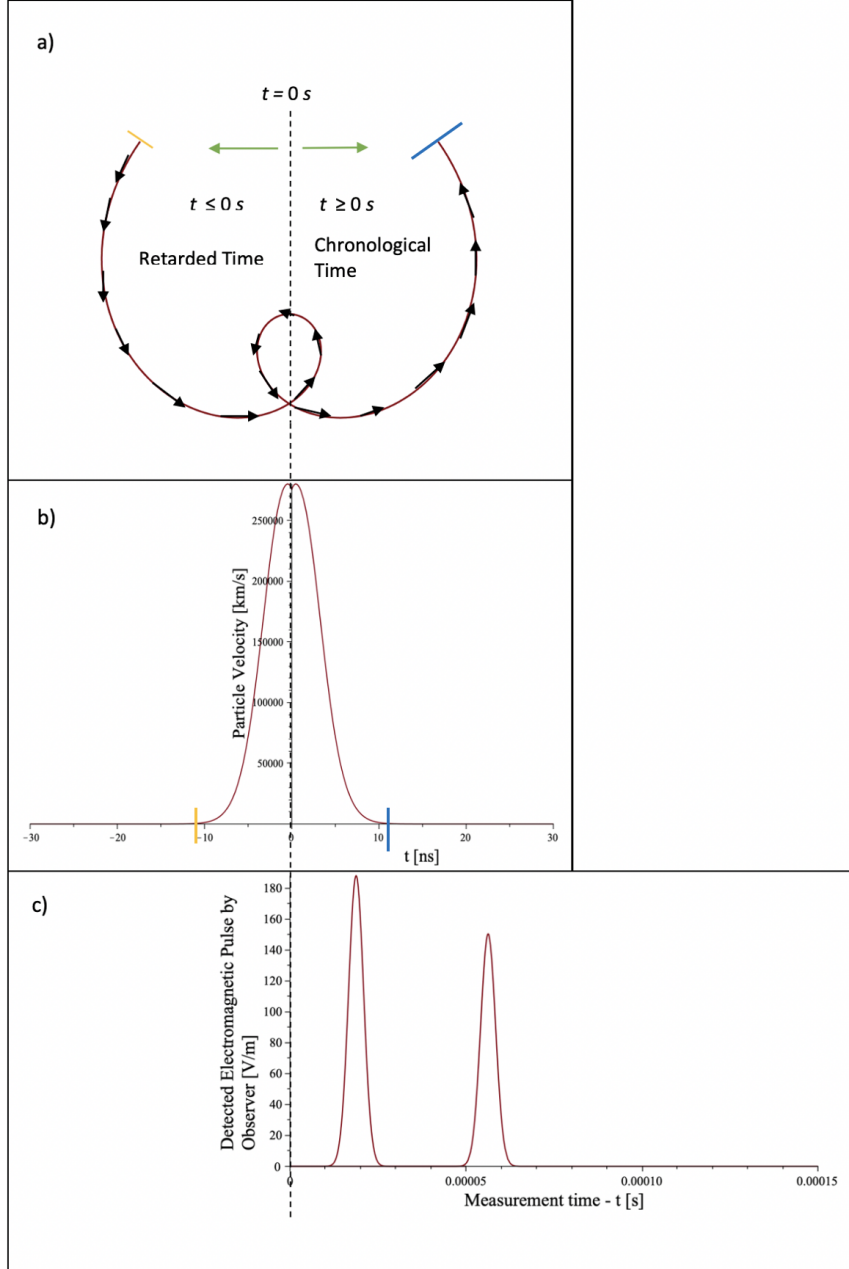
–11–

The relative particle velocity is

$$\beta(t) = \frac{v(t) + \frac{dr}{dt}}{c}.$$ (10)

Hence,

$$\beta(t) = \frac{s_{fv}s_f z(s_{ft})^{1.461}}{c} \frac{4.365 \times 10^{26}}{(1.333 \times 10^9 s_{ft} + 3.357 \times 10^{15}|s_{ftv}t|!)^{0.461}} - \frac{s_{fv}s_f z(s_{ft})^{1.5}}{c} \frac{1.565 \times 10^{27}}{((1.333 \times 10^9 s_{ft} + 3.357 \times 10^{15}|s_{ftv}t|!)^{0.5}} + \frac{dr}{dt}\frac{1}{c},$$ (11)

where t is the time in s and the range of the time changes in the velocity function (Eq. 9), hence in β (Eq. 11) function. The time range in velocity function differs from the electric field function given in equation 5 as a result of the integration process. The time range of the velocity function is $-\infty \le t \le \infty$. An important information to note about the indicated range of time t values separately in both, the scaled velocity function (Eq. 9) and the electric field function (Eq. 5), is that they are specific for this scaled velocity and non-scaled electric field function separately. There is no time parameter in any other equation nor in the final equation due to the nature of the definite integral of time. However, as indicated in equation 13, the definite integral between the limits of $-\infty$ and ∞ of time results in a time t parameter to vanish in the final equation (Eq. 43). Therefore, the range of time t values presented in sections 4 and 5 can be neglected for the final equation 43.

Before moving to the next section, the concepts explained so far make up the base of the complete theory. The next section uses the information of sections 2, 4, and 5 to construct the core of the theory and to derive the novel generic radiation intensity pattern of a single particle unique to the bremsstrahlung process. Figure 5 shows how this theory fits into practical observations.

Figure 5. Complete order of events from initial particle acceleration until pulse detection by an observer. a) The yellow line indicates the particle's starting position. It starts accelerating from -10 ns until $t = 0$ s as a result of an external leader tip electric field and Coulomb electric field (Bremsstrahlung) of the target particle in the atmosphere. b) Shows how the particle's velocity changes as a function of time. The particle is still allowed to propagate to positive time values. However, the starting time is from negative time values (retarded time). Negative time is required to reflect the reality that when the signal is measured by an observer at $t = 0$ s, it has to travel some time from the source to the observer. The acceleration process that causes the emission also requires some time to take place. The observer in chronological time does not observe all of these processes. Hence, they occur in negative retarded time. c) Sketches when the observer would receive the signal. It is plotted using the Dirac Delta function to sketch when the observer would receive the signal, which does not reflect the actual timing. The first signal could also be received at $t = 0$ s, however not in retarded time as it would then contradict the observations where there is no negative time.

–13–

6 Mathematical Model of Combined High and Low-Frequency Bremsstrahlung Radiation Pattern

Deriving the bremsstrahlung radiation pattern.

This section introduces collision cross-sections as a part of explaining complete radiation pattern. Further information on collision cross-section and mathematical definitions consisting of form factors can be found in supplemental information file in the form of text, S2 (Punjabi & Perdrisat, 2014). Collision cross-section and form factors are very important in defining the final form of the radiation patterns at high frequency (Perdrisat et al., 2007). Form factors are not used in the final equation and in simulations of radiation patterns. For high-frequency emissions, the details of collision and interaction are crucial. They are accounted for by adding a cross-section of a particle of interest.

Hence, it is assumed that

$$\frac{d^3\chi}{d\omega' d\Omega_{rad} d\Omega_{par}} = \frac{d^2 I}{d\omega' d\Omega_{rad}} \frac{d\sigma}{d\Omega_{par}}. \tag{12}$$

Dimensionally, $\chi = I \times \sigma$, where, σ in m^2 is the Coulomb scattering cross section, χ in Js^{-1}m^2 is the radiation cross section, and I in Js^{-1} is the radiation intensity. As a result of LinardWiechert potentials, the radiation emitted by a single charged particle (Jackson, 1999, p.675) is given by

$$\frac{d^2 I}{d\omega' d\Omega_{rad}} = \frac{z^2 e^2 (\omega')^2}{4\pi^2 c \epsilon_0} \left| \zeta \right|^2, \tag{13}$$

where $\zeta = \int_{-\infty}^{\infty} n \times (n \times \beta) e^{i\omega'(t - \vec{n}.r(t)/c)} dt$. In addition, z is the dimensionless charge number , c is the speed of light, ϵ_0 is the permittivity of free space, ω' is the angular frequency of the emitted wave in rad/s in the particle's frame of reference and t is the time in s.

The radiation unit vector n, the position vector $r(t)$ in equation 1, the particle motion, the position of an observer, and the overall theoretical concept about the bremsstrahlung radiation emission modeling that the equations are built upon are shown in the Figure 2.

As n is a unit vector in the direction of the emitted radiation, the integrand of the integral in equation (13) can be re-written in the sinusoidal form of the cross-product as

$$\zeta = \int_{-\infty}^{\infty} |\beta| |sin(\theta_{n,\beta})| e^{i\omega(t - \vec{n}.r\vec{(t)}/c)} dt, \tag{14}$$

or in the sinusoidal form of dot product as

$$\zeta = \int_{-\infty}^{\infty} |\beta| |sin(\theta_{n,\beta})| e^{i\omega(t - r(t) cos(\theta_{n,r(t)})/c)} dt. \tag{15}$$

Substituting equation (1) and the first term of equation (11) into equation (14) and taking constants out results in

–14–

$$\zeta = \frac{s_{fv}s_f z(s_{ft})^{1.461}4.365\times10^{26}}{c}sin(\theta_{n,\beta})\int_{-\infty}^{\infty}\frac{1}{(1.333\times10^9 s_{ft}+3.357\times10^{15}|s_{ftv}t|!)^{0.461}}$$
$$e^{i\omega(t-\left[\frac{(t^R)^2{}_bR_{(\omega')}R_{cos(\theta_{n,r(t)})}R_c}{\tau2R_cR\omega'cos(\theta_{n,r(t)})}-\frac{at}{\tau}\right]cos(\theta_{n,r(t)})/c)}dt. \tag{16}$$

A variable transformation from t to s requires the Jacobian. Assuming that $s = -t$ it follows that $\frac{ds}{dt} = -1$ such that

$$\zeta = -\frac{s_{fv}s_f z(s_{ft})^{1.461}4.365\times10^{26}}{c}sin(\theta_{n,\beta})\int_{-\infty}^{\infty}\frac{1}{(1.333\times10^9 s_{ft}+3.357\times10^{15}|s_{ftv}(-s)|!)^{0.461}}$$
$$e^{i\omega(-s-\left[\frac{((-s)^R)^2{}_bR_{(\omega')}R_{cos(\theta_{n,r(t)})}R_c}{\tau2R_cR\omega'cos(\theta_{n,r(t)})}-\frac{a(-s)}{\tau}\right]cos(\theta_{n,r(t)})/c)}ds. \tag{17}$$

The exponential term can be simplified such that

$$e^{-i\omega s}e^{-i\omega\frac{((-s)^R)^2{}_bR_{(\omega')}R_{cos(\theta_{n,r(t)})}R_c}{\tau2R_cR\omega'cos(\theta_{n,r(t)})}cos(\theta_{n,r(t)})/c}e^{-i\omega\frac{as}{\tau}cos(\theta_{n,r(t)})/c}. \tag{18}$$

Further simplification of the common parameters results in

$$e^{-i\omega s}e^{-i\frac{((-s)^R)^2{}_bR_{(\omega')}R_{cos(\theta_{n,r(t)})}R}{\tau2R_cR}}e^{-i\omega\frac{as}{\tau}cos(\theta_{n,r(t)})/c}, \tag{19}$$

where $e^{-i\omega s}$ can be neglected as there is no $\frac{1}{c}$ term to reduce the rate of exponential decay. Therefore, this term goes to zero quickly with time such that

$$e^{-i\frac{((-s)^R)^2{}_bR_{(\omega')}R_{cos(\theta_{n,r(t)})}R}{\tau2R_cR}}e^{-i\omega\frac{as}{\tau}cos(\theta_{n,r(t)})/c}. \tag{20}$$

Bringing the whole integral in equation (16) together with the simplified exponential gives

$$\zeta = -\frac{s_{fv}s_f z(s_{ft})^{1.461}4.365\times10^{26}}{c}sin(\theta_{n,\beta})\int_{-\infty}^{\infty}\frac{1}{(1.333\times10^9 s_{ft}+3.357\times10^{15}|s_{ftv}(-s)|!)^{0.461}}$$
$$e^{-i\frac{((-s)^R)^2{}_bR_{(\omega')}R_{cos(\theta_{n,r(t)})}R}{\tau2R_cR}}$$
$$e^{-i\omega\frac{as}{\tau}cos(\theta_{n,r(t)})/c}ds. \tag{21}$$

Finally, the velocity equation (9) converging to 0 m/s at $\mp\infty$ (see Figure 4.b) enables the integral in equation 21 to be evaluated. Convergence is due to the nature of derived electric field function, which goes to zero at infinite time and does not accelerate the particle any more. Furthermore, the use of functions such as Planck's radiation curve, Heidler current (Heidler et al., 2013), or Poisson distribution function with a variable transform to represent electric field would not be beneficial in deriving a velocity function as they diverge due to their exponential nature. The solution to the integral

–15–

is approximated by the use of a formula in the book of Fourier transforms of exponential functions (Bateman et al., 1954, p.121, eq. 23). The integral can be approximated by seeking a solution from the table of integral transforms by Harry Bateman for the exponential Fourier transform of the function $f(x) = f(s)$ being equal to

$$f(s) = \frac{1}{(1.333 \times 10^9 s_{ft} + 3.357 \times 10^{15} |s_{ftv}(-s)|!)^{0.461}} e^{i\alpha^2 s^2}. \tag{22}$$

The solution of the integral requires index ν in the variable $(ix)^\nu$ that multiplies the exponential function in Exponential Fourier Transform of function $f(x) = f(s)$ to be $\nu > -1$ (Bateman et al., 1954, p.121, eq. 23). The derivation of the velocity (Eq. 9) results in the beta function (Eq. 11) satisfying this requirement.

As the integrand of the integral in equation 14 multiplies with the β function consisting of 2 terms given in equation 11, the integral can be separated and solved individually for each term such that all terms can be added together to give the final result.

Hence, the approximated solution of the integral ζ for the first term of the scaled velocity function (11) β is $\nu_1 = -0.461 > -1$ such that

$$\frac{d^2 I}{d\omega \Omega_{rad}} = -\frac{s_{fv} s_f z (s_{ft})^{1.461} 4.365 \times 10^{26}}{c} \left[\pi^{1/2} 2^{-(1/2)\nu_1} \alpha^{-\nu_1 - 1} e^{-\frac{y^2 \alpha^{-2}}{8}} \times D_{\nu_1} (2^{-1/2} \alpha^{-1} y) \right]. \tag{23}$$

The approximated solution of the integral ζ for the second term of the scaled velocity function (11) β is $\nu_2 = -0.5 > -1$ such that

$$\frac{d^2 I}{d\omega \Omega_{rad}} = \frac{s_{fv} z s_f (s_{ft})^{1.5} 1.565 \times 10^{27}}{c} \left[\pi^{1/2} 2^{-(1/2)\nu_2} \alpha^{-\nu_2 - 1} e^{-\frac{y^2 \alpha^{-2}}{8}} \times D_{\nu_2} (2^{-1/2} \alpha^{-1} y) \right], \tag{24}$$

where $\alpha^2 = \frac{b^R (\omega')^R (cos(\theta_{n,r(t)}))^R}{(\tau^R)^2 c^R}$ $[s^{-2}]$ and $y = \frac{\omega' cos(\theta_{n,r(t)}) a}{c\tau}$ $[s^{-1}]$.

Therefore, the final radiation pattern for both high and low-frequency emission is the sum of the two terms

$$\frac{d^2 I}{d\omega' \Omega_{rad}} = \frac{z^2 e^2 (\omega')^2}{4\pi^2 c \epsilon_0} \left| sin(\theta_{n,\beta}) \left[-\frac{s_{fv} s_f z (s_{ft})^{1.461} 4.365 \times 10^{26}}{c} \right.\right.$$
$$\left[\pi^{1/2} 2^{-(1/2)\nu_1} \alpha^{-\nu_1 - 1} e^{-\frac{y^2 \alpha^{-2}}{8}} \times D_{\nu_1} (2^{-1/2} \alpha^{-1} y) \right] + \tag{25}$$
$$\left.\left. \frac{s_{fv} z s_f (s_{ft})^{1.5} 1.565 \times 10^{27}}{c} \left[\pi^{1/2} 2^{-(1/2)\nu_2} \alpha^{-\nu_2 - 1} e^{-\frac{y^2 \alpha^{-2}}{8}} \times D_{\nu_2} (2^{-1/2} \alpha^{-1} y) \right] \right] \right|^2,$$

where R is the bremsstrahlung asymmetry control parameter, which plays a crucial role in distinguishing the parameter y from α, which is a requirement in order to be able to approximate the solution to an integral (dimensionless). $D_v(z)$ is the parabolic cylinder function.

The parabolic cylinder function is given by (Whittaker & Watson, 1927, p. 347)

$$D_v(z) = 2^{v/2 + 1/4} z^{-1/2} W_{v/2 + 1/4, 1/4} (1/2 z^2), \tag{26}$$

–16–

where, $W_{v/2+1/4,1/4}(1/2z^2)$ is a Whittaker function (Whittaker & Watson, 1927, p. 346) and

$$W_{\kappa,\mu}(1/2z^2) = \frac{\Gamma(-2\mu)M_{\kappa,\mu}(1/2z^2)}{\Gamma(1/2-\mu-\kappa)} + \frac{\Gamma(2\mu)M_{\kappa,-\mu}(1/2z^2)}{\Gamma(1/2+\mu-\kappa)}, \tag{27}$$

where, $M_{\kappa,\mu}(1/2z^2)$ is another Whittaker function (Kiyosi Ito and The Mathematical Society of Japan, 1993) & (Whittaker & Watson, 1927, p. 347) and

$$M_{\kappa,\mu}(1/2z^2) = {}_1F_1(1/2+\mu-\kappa; 2\mu+1; 1/2z^2)(1/2z^2)^{1/2+\mu}e^{-1/21/2z^2}. \tag{28}$$

For the second term of equation (27) with Whittaker M function of negative μ

$$M_{\kappa,-\mu}(1/2z^2) = {}_1F_1(\mu-\kappa; 2\mu; 1/2z^2)(1/2z^2)^{1/2+\mu}e^{-1/21/2z^2}, \tag{29}$$

where ${}_1F_1(1/2+\mu-\kappa; 2\mu+1; z)$ is a confluent hypergeometric function of the first kind (Abramowitz & Stegun, 1972) and

$${}_1F_1(1/2+\mu-\kappa; 2\mu+1; 1/2z^2) = \frac{U_{\kappa,\mu}(1/2z^2)}{e^{-1/2z^2/2}(1/2z^2)^{\mu+1/2}}, \tag{30}$$

where, $U_{\kappa,\mu}(\frac{z^2}{2})$ is the confluent hypergeometric function of the second kind, named Kummer's U function such that

$$U_{\kappa,\mu}(\frac{z^2}{2}) = (\frac{z^2}{2})^{\mu+1/2}e^{-\frac{z^2}{4}}\sum_{n=0}^{\infty}\frac{(m-k+1/2)_n}{n!(2\mu+1)_n}\left(\frac{z^2}{2}\right)^n. \tag{31}$$

By direct comparison of equation 26 with 25 and equation 26 with 27, the constant quantities z, κ and μ are defined as $z = 2^{-1/2}\alpha^{-1}y$, $\kappa = v/2+1/4$, $\mu = 1/4$.

Finally, in order to complete equation 25, the observation angles ($\theta_{n,\beta}$ and $\theta_{n,r(t)}$) need to be reduced from two to one as they are related to each other.

Currently, the radiation pattern is observed from $cos(\theta_{n,r(t)})$ and $sin(\theta_{n,\beta})$. In addition, $cos(\theta_{n,r(t)})$ coming from substitute parameter α and y in equation 25 and $sin(\theta_{n,\beta})$ being a variable parameter in equation 25 defining the radiation around the particle, also known as the solid angle. In addition, by looking at the Figure 2b, it can be seen that the velocity vector, which is the derivative of the position vector $r(t)$ is always perpendicular to the position vector where radiation unit vector pointing in the direction of the emitted radiation makes up the hypotenuse of the formed rectangular triangle. Hence, the angles of the rectangular triangle can be equated to each other.

The velocity function defined in equation 9 provides the particle speed attained by the acceleration due to the external leader tip electric field, and it is scalar. The derivative of the position vector $r(t)$ (Eq. 1) provides the velocity caused by the Coulomb interaction of an incoming and target particle, which also determines the curved trajectory of the bremsstrahlung given by the position vector (Eq. 1). Hence, the particle's overall velocity moving perpendicular to the position vector $r(t)$ is the sum of the Coulomb velocity arising from the derivative of the position vector $r(t)$ plus the scalar speed attained by the external leader tip electric field given in equation 9. Equation 9 is not the velocity, but the speed. It only provides magnitude but gives no information about the direction of the particle's motion. The direction of the particle's motion is already provided by the position vector $r(t)$ given by equation 1. As a result

–17–

$$sin(\theta_{n,\beta}) = \frac{r(t)}{n} \tag{32}$$
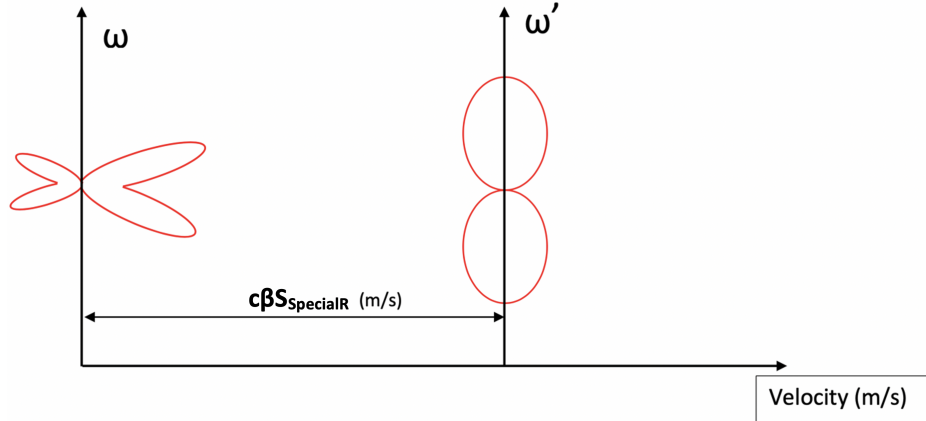
and

$$cos(\theta_{n,r(t)}) = \frac{r(t)}{n}, \tag{33}$$

such that

$$sin(\theta_{n,\beta}) = cos(\theta_{n,r(t)}). \tag{34}$$

7 Dynamic Bremsstrahlung - Special Relativity & Doppler effect

Now the Doppler shift is added to the emitted radiation.

Figure 6 displays a stationary laboratory frame ω where the relativistic effects and the Doppler shift is observed, particle's moving frame of reference ω' and the relative velocity $c\beta S_{SpecialR}$ between the observer and the two different frames that determines what an observer would detect. In addition, $S_{SpecialR}$ (dimensionless) is a scaling factor of the relative velocity between the two different frames of references. In particular, $S_{SpecialR} = 1$ means the observer is stationary, and the particle is propagating at its velocity. As the $S_{SpecialR}$ approaches zero, the relative velocity between the observer and the particle falls, meaning that the observer is getting closer to the particle's velocity and would start to observe or detect a non-relativistic dipole radiation pattern.

Figure 6. Particle radiation at two different frames of references. Laboratory (stationary) frame of reference ω and moving frame of reference ω' with the velocity $c\frac{v(t)}{c}S_{SpecialR}$. In addition, $S_{SpecialR} = 0$ meaning the observer is moving with the particle at the same velocity at all times, hence would see no radiation emission as the particle is not accelerating. As $S_{SpecialR} \to 0$, the observer would see dipole radiation pattern. As $S_{SpecialR} \to 1$, the observer would approach rest and would see the particle propagating at its own velocity defined by equation (9) with the corresponding radiation pattern.

The equation for translating the angular frequency of the emitted wave into the laboratory frame for the Doppler shift is given by (Jackson, 1999, p. 720, eq. 15.40).

$$\omega' = \gamma\omega(S_{SpecialR} - \beta S_{SpecialR}cos(\theta_{n,\beta})). \tag{35}$$

–18–

449 As shown in Figure 2b, $\theta_{n,\beta}$ is the angle between the emitted radiation unit vec-
450 tor and the particle velocity vector.

451 Substituting equation 34, and 35 into the equation 25 gives

$$
\frac{d^2I}{d\omega\Omega_{rad}} = \frac{z^2e^2(\gamma\omega(S_{SpecialR} - \beta S_{SpecialR}cos(\theta_{n,\beta}))^2}{4\pi^2c\epsilon_0}\left|sin(\theta_{n,\beta})\left[-\frac{s_{fv}s_fz(s_{ft})^{1.461}4.365\times10^{26}}{c}\right.\right.
$$
$$
\left[\pi^{1/2}2^{-(1/2)\nu_1}\alpha^{-\nu_1-1}e^{-\frac{y^2\alpha^{-2}}{8}}\times D_{\nu_1}(2^{-1/2}\alpha^{-1}y)\right]+
$$
$$
\left.\left.\frac{s_{fv}zs_f(s_{ft})^{1.5}1.565\times10^{27}}{c}\left[\pi^{1/2}2^{-(1/2)\nu_2}\alpha^{-\nu_2-1}e^{-\frac{y^2\alpha^{-2}}{8}}\times D_{\nu_2}(2^{-1/2}\alpha^{-1}y)\right]\right]\right|^2,
$$
$$
\tag{36}
$$

452 where the Lorentz factor γ is $\gamma = \frac{1}{\sqrt{1-\beta^2}}$ (dimensionless), and ω is the received an-
453 gular frequency in the laboratory (stationary) frame of reference in rad/s. In addition,
454 the new definition of α is $\alpha^2 = \frac{b^R(\gamma\omega(S_{SpecialR} - \beta S_{SpecialR}cos(\theta_{n,\beta})))^R(sin(\theta_{n,\beta}))^R}{(\tau^R)^2c^R}$ $[s^{-2}]$, and
455 the new definition of y is $y = \frac{\gamma\omega(S_{SpecialR} - \beta S_{SpecialR}cos(\theta_{n,\beta}))sin(\theta_{n,\beta})a}{c\tau}$ $[s^{-1}]$.

456 The scaling factor s_f in equation 36 is carried over from the definition of the electric field equation 5.
457 As a result of the integration process, s_f scales the magnitude of the emitted radiation, which is directly
458 linked with its previous purpose of scaling the electric field, which defines the magnitude of the emitted
459 radiation. The scaling factor s_f can be approximated at high frequency with a scalar equa-
460 tion that gives the magnitude of the emitted high-frequency radiation from a single par-
461 ticle in an instantaneous circular motion (Jackson, 1999, p. 679, eq. 14.84).

462 Hence,

$$
s_f \simeq \frac{\frac{d^2I}{d\Omega d\omega}|_{\theta=0}}{|\frac{d^2I}{d\Omega d\omega}|} \simeq \frac{\frac{3e^2\gamma^2\omega e^{\frac{-\omega}{\omega_c}}}{4\pi c\omega_c}}{|\frac{d^2I}{d\Omega d\omega}|}
\tag{37}
$$

463 and the critical angular frequency (Jackson, 1999, p. 679, eq. 14.81) is

$$
\omega_c = \frac{3\gamma^3}{2}\left(\frac{c}{p}\right),
\tag{38}
$$

464 where p is the radius of curvature of instantaneous circular motion in m, ω_c is the
465 critical angular boundary frequency. Beyond critical angular boundary frequency, the
466 emitted radiation would have a minimal value in all directions such that it can be ne-
467 glected.

8 Results

469 This section presents predictions of radiation patterns of a single electron accelerated under an
470 external lightning leader tip electric field using the derived equation 36.

471 Radiation patterns change as a result of changing particle velocity, and accelera-
472 tion as a particle get relativistic. As the acceleration of a charged particle increases, it
473 emits higher intensity, hence higher frequency radiation. Therefore, the input param-
474 eter, emitted radiation frequency represents particle acceleration. To simulate relativis-
475 tic and non-relativistic radiation patterns, the range of input velocity and frequency val-
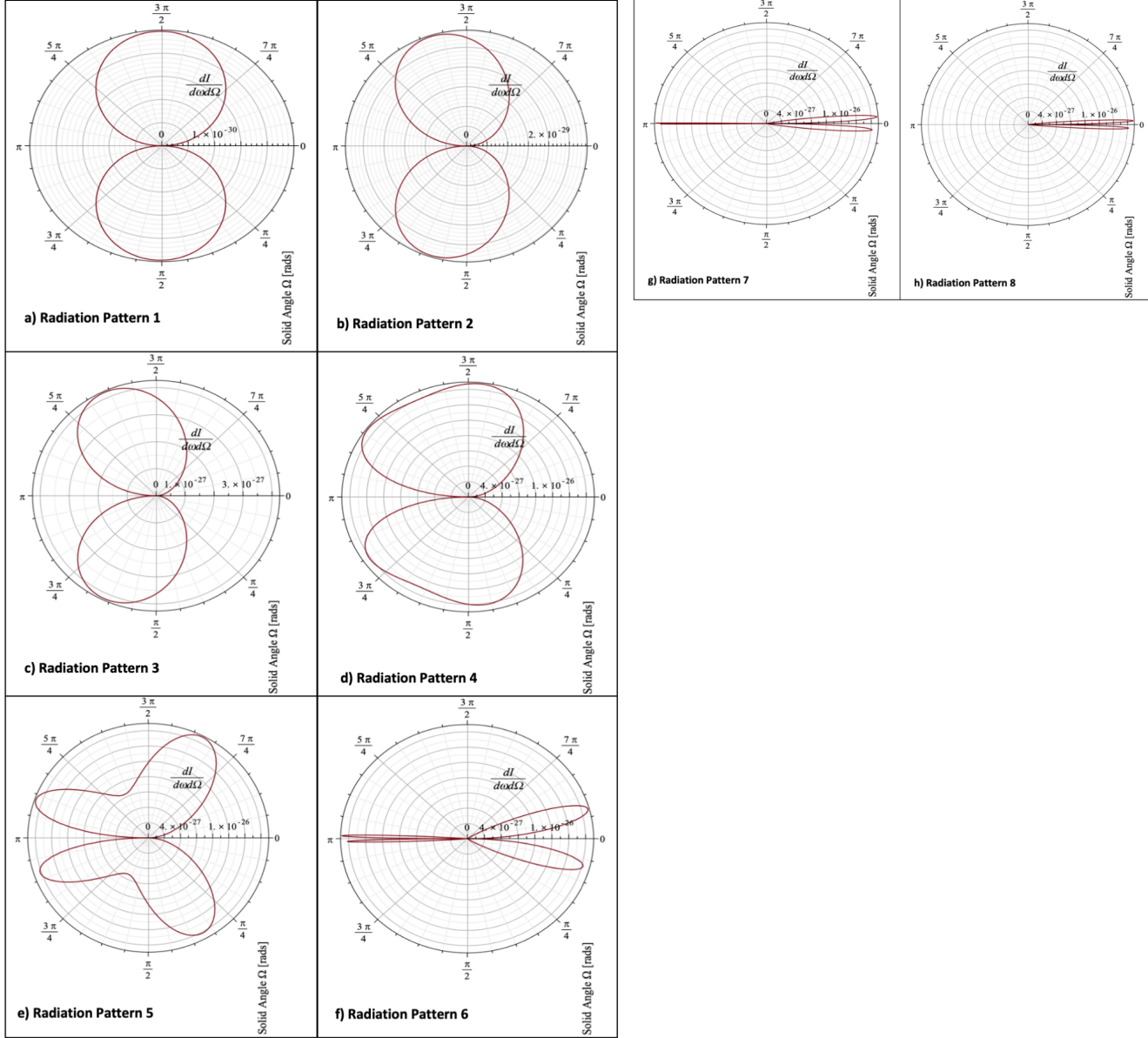476 ues were chosen and tabulated in table 1.

Velocity is shown as ratio with the speed of light β and emitted radiation frequency (Hz)		
Radiation Patterns	Scaled Bremsstrahlung Electron Velocity β (Dimensionless)	Emitted Radiation Frequency (Hz)
Pattern 1	0.02	1 k
Pattern 2	0.36	10 k
Pattern 3	0.67	1 M
Pattern 4	0.69	7 M
Pattern 5	0.77	10 M
Pattern 6	0.85	100 M
Pattern 7	0.87	500 M
Pattern 8	0.90	1 G

Table 1. Radiation pattern input parameters are velocity as a ratio to the speed of light β, and emitted radiation frequency by the particle for eight different radiation patterns. Emitted radiation frequency by a single particle is an input parameter to the final equation (36). It plays a crucial role in delivering valuable information and determining the particle's total acceleration, hence the total velocity is indirect as there is no input acceleration parameter in the final equation 36. In addition, β function determines the particle's total velocity arising significantly from the external lightning leader tip electric field. The remaining contribution to the overall velocity comes from the Coulomb force between an incoming and target particle, where the target particle causes an incoming particle to follow and covers some arc length of the spiral trajectory described in the position vector (Eq. 1) during its mean free time of the collision.

477   The new radiation patterns reveal that as well as forward peaking, there are also backward peaking
478 lobes as the particle gains speed. The magnitude of the acceleration determines the magnitude of the
479 radiation intensity. The horizontal axis is the radiation intensity per solid angle per emitted frequency range
480 in eight different radiation patterns displayed in Figure 7. Although there is overall more energy in the forward
481 peaking lobes, the peak radiation intensity in the backward direction is slightly higher in patterns 5, 6, and 7
482 as they are more horizontally projected. However, the total radiation intensity is higher in the forward
483 direction as the peaking lobes have larger beam areas due to the Doppler effect's presence.

484   The peak intensity of the backward lobes starts to decay as a result of the Doppler shift from pattern
485 seven onwards. The Doppler shift effect can be observed from the consideration of both radiation length
486 in the horizontal direction (as the horizontal axis is a measure of the radiation intensity per solid angle,
487 i.e., more horizontally projected) and the total area of the emitted radiation pattern. The larger the area
488 of the radiation pattern, the more the beam extends in the horizontal direction or, when it is more projected
489 towards the horizontal axis, the more energy the emitted wave has. An increasing particle velocity
490 translates into increasing radiation frequency. Therefore an increase in energy in the forward direction
491 of the particle lowers the frequency and hence lowers the energy at the backward direction of the particle
492 due to the Doppler effect. For example, in the eighth radiation pattern, which is at $\sim 94\%$ of the speed of light
493 and has 1 GHz frequency, increasing the frequency of the observed radiation leads to an increase in the Doppler
494 effect that reduces the frequency, hence the energy ($E = hf$) of the beam at the back of the particle.
495 As a consequence, backward radiation lobes start to shrink such that overall radiation
496 pattern looks like a basic forward peaking radiation pattern (the pattern 8).
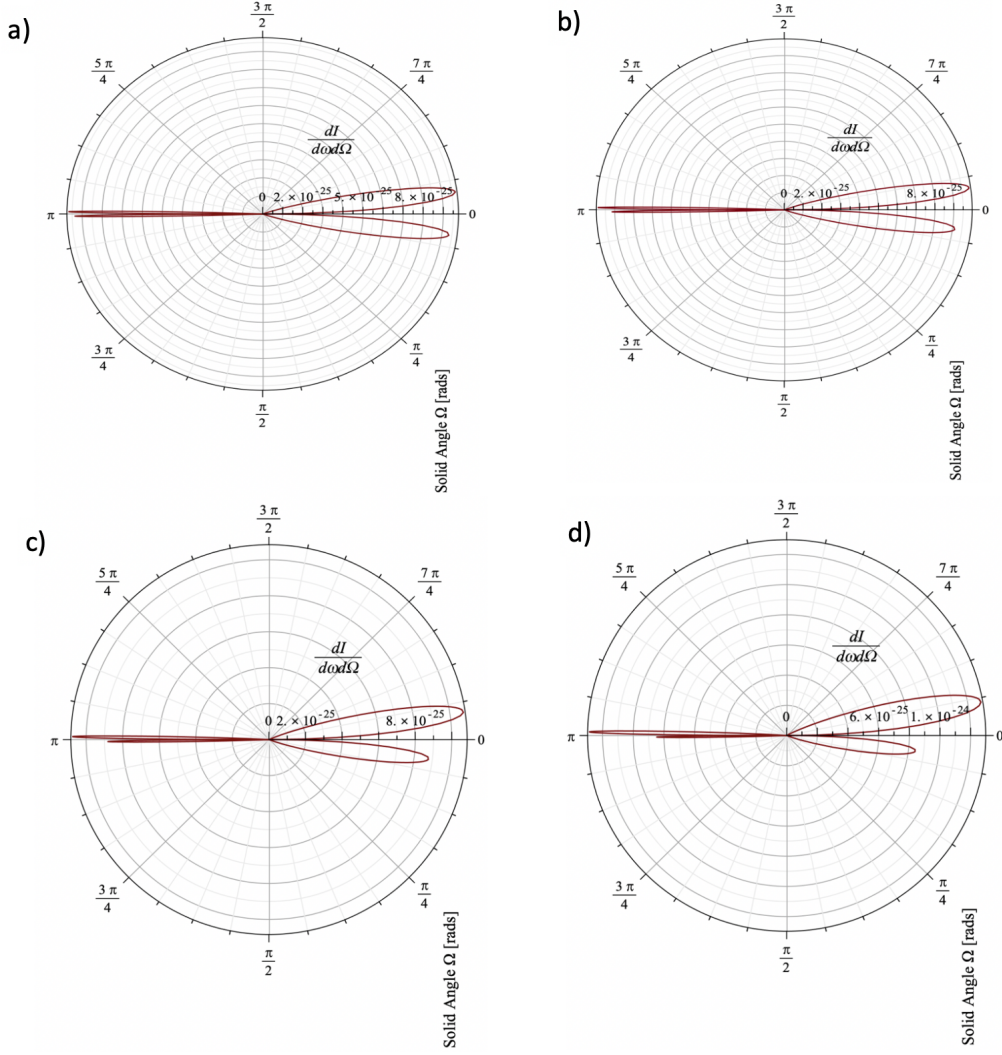
Figure 7. The Radiation patterns emitted by anti-clockwise rotating charged particle - bremsstrahlung process. Plot is in Polar co-ordinates. Horizontal axis gives the radiation intensity per Solid angle, Ω, per emitted angular radiation frequency, ω. In addition, angle of the Polar plot is the Solid angle, Ω. a-f) The radiation pattern connecting dipole with a forward-backward peaking radiation pattern is called the transition pattern. The radiation patterns and formula explaining the radiation patterns is not complete if it doesnt demonstrate the transition patterns. The transition patterns explain how the particle attains relativistic forward-backward peaking lobes. The radiation pattern of a particle during the bremsstrahlung, starting from a low velocity up until a relativistic velocity starts from the dipole radiation pattern and exhibits the forward and backward peaking radiation pattern. The transition is demonstrated in radiation patterns 4 and 5, where the dipole collapses to form four maxima. The values used for plotting are: mean free time $\tau = 30$ μs, number of charges $z = 1$, $a = 100$ μm, $b = 1$ nm (a and b are related to mean free path), $s_{ft} = 1$, $s_f = 1$, $S_{SpecialR} = 1$, velocity-time scaling factor $s_{ftv} = 1 \times 10^9$ and velocity scaling factor $s_{fv} = 8.19 \times 10^{-11}$. Finally, the bremsstrahlung asymmetry is $R = 1/8$. In addition, $\frac{1}{9} \leq R \leq \frac{1}{3}$. g) A particle reaching relativistic speed attains a focused beam in both forward and backward direction. h) A particle reaching to ultra-relativistic speed experiences the take over of the Doppler effect that minimizes the low-frequency radiation in the backward direction and emits almost fully in the forward direction.

–21–

Radiation patterns on the polar plot have to start from 2π rad until 0 rad to show the particle's complete radiation. Progression towards the zero is because a particle starts from the retarded time and radiates until the chronological time $t=0$ s and beyond, as shown in the Figures 2 and 5. If the polar plot were made with time as a representation of the solid angle, the plot would have started from $\sim$ -10 ns (when the particle starts accelerating, see the Figures 2 and 5) until 0 s. In addition, this is the same as starting from positive time and ending at $t = 0$ s. Therefore, the final result is independent of positive or negative start time as long as the time flow is towards zero seconds. The independence of the sign is caused by the absolute time and symmetry of the velocity function. Progression towards zero seconds is caused by the initial start time being retarded negative time.

The derived mathematical model (Eq. 36) is specifically for the bremsstrahlung process. Unlike many of the other radiation emission processes of charged particles (i.e., from linear acceleration or crossing the boundary between two different dielectric media), the bremsstrahlung process affects the shape of the emitted radiation. This bremsstrahlung effect causes an asymmetry of the emitted radiation about the particle's velocity vector or, in other terms, the direction of motion. To understand this effect, we can compare an electron to a car that travels in the dark with the headlight turned on. The headlights are the emitted electromagnetic radiation by the car. When the car gets into the bend, like the bremsstrahlung process of an electron, an observer outside the car can immediately tell the radiation shape of the headlight would be asymmetric by looking at the reflections on the road compared to the case when the car follows a straight path. This novel effect is clearly shown in supporting information in the Figure S1, which displays a real-life example of visible asymmetry of the car headlights (electromagnetic radiation) on a bend.

Figure 8 displays the effects of the bremsstrahlung radiation asymmetry control quantity R. The bremsstrahlung asymmetry R depends on the radius of the curvature of the incoming particle trajectory undergoing the bremsstrahlung process. In addition, the bremsstrahlung asymmetry R increases as the radius of curvature of the bremsstrahlung trajectory decreases.

Figure 8. Bremsstrahlung Asymmetry Quantity R with different values. a) $R = \frac{1}{9}$, b) $R = \frac{1}{6}$, c) $R = \frac{1}{4}$, d) $R = \frac{1}{3}$

9 Discussion

Firstly, the created model describing radiation patterns specifically for the bremsstrahlung process is modeled to be generic and applicable to all bremsstrahlung process on earth, outer space, or other planets. As mentioned in the third paragraph of the introduction, TGFs are believed to originate as a result of the bremsstrahlung process of RREA driven by external leader tip electric field. Hence, the theoretical model assumes a single particle accelerated under an external leader tip electric field interacting with a target particle or ion via Coulomb field. In addition, the incoming particle is assumed to follow a spiral particle trajectory. This assumption is based on the in-balance of centripetal (Coulomb field between two particles + Earth's external magnetic field) and centrifugal (external leader tip electric field) forces acting on the incoming particle when it interacts with a target particle via Coulomb field. Any in-balance in centripetal and centrifugal force acting on an incoming particle that follows a curved trajectory would result in a spiral particle trajectory. Hence, the choice of spiral trajectory considers the effects of the Earth's external magnetic field, B on an incoming particle trajectory in an indirect way.

–23–

Particle speed defined in equation (9) relies on the ansatz of a sharp rise and slow decay form of leader tip electric field. This ansatz originates and is backed up by the asymmetric γ-ray bursts (GRBs) measurement that reveals the internal charge structure of the leader tip described in the introduction section, in the second paragraph.

Although acceleration is modeled from the electric field that assumes the same behavior as the leader tip electric field observed in the atmosphere, it only provides a magnitude component of the electric field acceleration. Independent input parameters such as particle trajectory, the bremsstrahlung asymmetry, R, and the Doppler effect are fundamental physics where the particle trajectory, and the bremsstrahlung asymmetry, R are specific to the bremsstrahlung process. These input parameters enable the created model to apply to any bremsstrahlung processes.

The bremsstrahlung process has a continuous electromagnetic spectrum meaning it is capable of explaining both ionizing and low-frequency radiations. The bremsstrahlung radiation patterns presented in figure 7 are unique to a bremsstrahlung process. They are always the same in geometry with forward-backward radiation patterns at relativistic particle speeds and all the asymmetries. However, when the model is applied to any other bremsstrahlung processes other than Terrestrial-Gamma ray flashes (TGFs), only radiation intensities are subject to change but not the radiation shapes.

Overall, the eight different radiation patterns plotted in Figure 7 are not the complete radiation patterns, especially for high-frequency radiation. As mentioned in the previous section, a high-frequency radiation pattern is sensitive to the interaction process described by scattering cross-sections that an incoming bremsstrahlung electron experiences against target particles. Moreover, plotted radiation patterns are the second-order derivative term $\frac{d^2 I}{d\omega d\Omega_{rad}}$ of the equation (12), and it misses the information of interaction described by Coulomb scattering cross-section. In future work, a complete radiation pattern will be calculated using the complete equation (12), (36), and equation (1) provided in the supplemental information, S2 with appropriate form factors, and a dimensional analysis to describe high-frequency emissions. Furthermore, the first part of the derived equation demonstrates a success as Figures 7a (patterns 1) and 7h (pattern 8), display the common expected radiation patterns such as low-frequency dipole radiation pattern and relativistic forward peaking radiation patterns (Jackson, 1999, p. 669, Fig. 14.4).

The dipole radiation pattern 1 in Figure 7a displays perfect symmetry about both the velocity axis and the axis perpendicular to the velocity vector. In the absence of a Doppler and bremsstrahlung asymmetric radiation effect, the four maxima of the relativistic radiation pattern are symmetric about both the velocity axis and the axis perpendicular to the velocity. Therefore, following the statement of Noether's theorem, conservation of energy arising from the symmetry in the radiation lobes about the two axes mentioned above, causes the dipole radiation pattern 4 and 5 (in Figure 7d, 7e) to collapse and form 4 symmetric maxima. Initially, there were symmetries about two axes, and as the particle gains up speed, the number of symmetric axes should still be preserved. Hence, if there is only a forward peaking radiation with none in the backward direction, one of the symmetry is broken (about axes perpendicular to the velocity). The idea of preserving the initial number of symmetric axes is quite powerful in understanding why there are four maxima (two forward peakings and two backward peakings) and why the dipole collapses to form 4 maxima of the radiation pattern. All the radiation patterns in Figure 7 incorporate the Doppler effect and the bremsstrahlung trajectory asymmetry. These two effects cause the radiation pattern to be asymmetric. However, the emitted total radiation energy is still conserved compared between the presence and absence of radiation pattern asymmetry causing physical effects (The bremsstrahlung trajectory and the Doppler effect) at any given particle velocity. In other words, the total energy radiated at a given velocity is the same regardless of the Doppler and the bremsstrahlung trajectory effect. While these two effects increase the radiation beam intensity in one di-

rection, they also decrease the radiation intensity in other directions by the same amount such that the overall energy radiated by the particle at a given speed remains the same.

On the other hand, the reported radiation asymmetry of the bremsstrahlung (R-parameter) about the velocity vector due to the particle's curved trajectory was found to be existing at relativistic speeds when forward and backward peaking radiation patterns are present. This bremsstrahlung radiation asymmetry (R - parameter) we get is a novel finding. At the non-relativistic speeds, when radiation has a dipole pattern, asymmetry of the bremsstrahlung was found to be absent. This absence indicates that asymmetry is associated with being a physical effect rather than a mathematical artifact. The absence of the bremsstrahlung radiation asymmetry at a non-relativistic dipole radiation pattern of a particle following a curved trajectory can again be compared to a car having its headlights on each side of the door radiating perpendicular with respect to the velocity vector of the car. In this case, one can see that two emitted radiation beams would not be asymmetric as two beams are in the opposite direction to each other and are independent of the curvature of the trajectory as headlights radiate perpendicular to the trajectory.

Asymmetries are important because they alter the radiation intensity of the emitted radiation. Asymmetries increase the radiation intensity in one direction and decrease it in the other direction. The bremsstrahlung radiation pattern of a single particle with involved asymmetries can be used with a Monte Carlo simulation for multiple particles to predict radiation intensity map across an area where lightning discharge takes place. The radiation intensity map is the expected radiation power at each different observation location around the area of lightning discharge location. The predicted radiation intensity map allows improving the lightning detection and location systems. It helps to find the location of peak radiation intensity, hence contributes to the development of better radiation protection systems.

10 Summary

In summary, the radiation patterns were found to be peaking in a backward direction as well as an already known forward direction. In addition, four maxima (2 in the forward direction and 2 in the backward direction) were found to be due to the conservation of symmetry axes arising from the initial dipole radiation pattern. With the introduction of the Doppler effect, peaking lobes of radiation in forward and backward directions were found to be asymmetric about an axis perpendicular to the particle's velocity vector. Moreover, the novel second asymmetry of peaking lobes with respect to particle's velocity vector was found to be unique to the bremsstrahlung due to the particle following a curved trajectory. Finally, it is also found that low-frequency radiation peaks in the backward direction, whereas high-frequency peaks in forward direction.

References

Abramowitz, M., & Stegun, I. A. (1972). Handbook of Mathematical Functions: with Formulas, Graphs, and Mathematical Tables. In (10th ed., Vol. National Bureau of Standards Applied mathematics series 55, p. 1046). Washington, D.C. , USA: U.S. Dept. of Commerce : U.S. G.P.O. (ISBN: 9781591242178)

Babich, L. P., Bochkov, E. I., & Kutsyk, I. M. (2014). Mechanism of generation of runaway electrons in a lightning leader. *JETP Letters*, *99*(7), 386–390. Retrieved from https://doi.org/10.1134/S0021364014070029 doi: 10.1134/S0021364014070029

Babich, L. P., Bochkov, E. I., Kutsyk, I. M., Neubert, T., & Chanrion, O. (2015a). A model for electric field enhancement in lightning leader tips to levels allowing X-ray and ray emissions. *Journal of Geophysical Research: Space Physics*, *120*(6), 5087-5100. Retrieved from https://agupubs.onlinelibrary.wiley.com/doi/abs/10.1002/2014JA020923 doi: 10.1002/2014JA020923

Babich, L. P., Bochkov, E. I., Kutsyk, I. M., Neubert, T., & Chanrion, O. (2015b). A model for electric field enhancement in lightning leader tips to levels allowing xray and ray emissions. *Journal of geophysical research.*, *120*(6), 5087–5100. doi: 10.1002/2014JA020923

Bateman, H., W.Magnus, F.Oberhettinger, & F.G.Tricomi. (1954). Table of Integral Transforms. In (1st ed., Vol. 1, p. 121). New York, USA: McGraw-Hill Book Company,Inc. (ISBN:07-019549-8)

Bourilkov, D. (2000, Sep). Search for tev strings and new phenomena in bhabha scattering at cern lep2. *Phys. Rev. D*, *62*, 076005. Retrieved from https://link.aps.org/doi/10.1103/PhysRevD.62.076005 doi: 10.1103/PhysRevD.62.076005

Brock, C. P. (2019). Atomic form factors-international tables for crystallography. In (6th ed., Vol. C, p. 554-595). Hoboken, United States: Wiley. (ISBN:978-1-119-46870-7)

Celestin, S. (2016, December). Electron acceleration mechanisms in thunderstorms. *arXiv*, 1-6. doi: arXiv:1701.00105[astro-ph.HE]

Celestin, S., & Pasko, V. P. (2011). Energy and fluxes of thermal runaway electrons produced by exponential growth of streamers during the stepping of lightning leaders and in transient luminous events. *Journal of Geophysical Research: Space Physics*, *116*(A3). Retrieved from https://agupubs.onlinelibrary.wiley.com/doi/abs/10.1029/2010JA016260 doi: 10.1029/2010JA016260

Chanrion, O., & Neubert, T. (2010). Production of runaway electrons by negative streamer discharges. *Journal of Geophysical Research: Space Physics*, *115*(A6), 1-10. Retrieved from https://agupubs.onlinelibrary.wiley.com/doi/abs/10.1029/2009JA014774 doi: 10.1029/2009JA014774

Connaughton, V., Briggs, M. S., Xiong, S., Dwyer, J. R., Hutchins, M. L., Grove, J. E., . . . Wilson-Hodge, C. (2013, May). Radio signals from electron beams in terrestrial gamma ray flashes. *Journal of Geophysical Research: Space Physics*, *118*(5), 2313-2320. Retrieved from https://agupubs.onlinelibrary.wiley.com/doi/abs/10.1029/2012JA018288 doi: 10.1029/2012JA018288

Cummer, S. A., Briggs, M. S., Dwyer, J. R., Xiong, S., Connaughton, V., Fishman, G. J., . . . Solanki, R. (2014, December). The source altitude, electric current, and intrinsic brightness of terrestrial gamma ray flashes. *Geophysical Research Letters*, *41*(23), 8586-8593. Retrieved from https://agupubs.onlinelibrary.wiley.com/doi/abs/10.1002/2014GL062196 doi: 10.1002/2014GL062196

Dwyer, J. R. (2007). Relativistic breakdown in planetary atmospheres. *Physics of Plasmas*, *14*(4), 042901. Retrieved from https://doi.org/10.1063/1.2709652 doi: 10.1063/1.2709652

Dwyer, J. R. (2008). Source mechanisms of terrestrial gamma-ray flashes. *Journal of*

Geophysical Research: Atmospheres, *113*(D10), 1-12. Retrieved from `https://agupubs.onlinelibrary.wiley.com/doi/abs/10.1029/2007JD009248` doi: 10.1029/2007JD009248

Dwyer, J. R., Smith, D. M., & Cummer, S. A. (2012a). High-energy atmospheric physics: Terrestrial gamma-ray flashes and related phenomena. *Space Science Reviews*, *173*(1), 133–196. Retrieved from `https://doi.org/10.1007/s11214-012-9894-0` doi: 10.1007/s11214-012-9894-0

Dwyer, J. R., Smith, D. M., & Cummer, S. A. (2012b, June). High-Energy Atmospheric Physics: Terrestrial Gamma-Ray Flashes and Related Phenomena. *Space Science Reviews*, *173*(1), 133–196. Retrieved from `https://doi.org/10.1007/s11214-012-9894-0` doi: 10.1007/s11214-012-9894-0

Fishman, G. J., Bhat, P. N., Mallozzi, R., Horack, J. M., Koshut, T., Kouveliotou, C., ... Christian, H. J. (1994). Discovery of intense gamma-ray flashes of atmospheric origin. *Science*, *264*(5163), 1313–1316. Retrieved from `https://science.sciencemag.org/content/264/5163/1313` doi: 10.1126/science.264.5163.1313

Foley, S., Fitzpatrick, G., Briggs, M. S., Connaughton, V., Tierney, D., McBreen, S., ... Wilson-Hodge, C. (2014, June). Pulse properties of terrestrial gamma-ray flashes detected by the Fermi Gamma-Ray Burst Monitor. *Journal of Geophysical Research: Space Physics*, *119*(7), 5931-5942. Retrieved from `https://agupubs.onlinelibrary.wiley.com/doi/abs/10.1002/2014JA019805` doi: 10.1002/2014JA019805

Grefenstette, B. W., Smith, D. M., Dwyer, J. R., & Fishman, G. J. (2008, March). Time evolution of terrestrial gamma ray flashes. *Geophysical Research Letters*, *35*(6), 1-5. Retrieved from `https://agupubs.onlinelibrary.wiley.com/doi/abs/10.1029/2007GL032922` doi: 10.1029/2007GL032922

Hariharan, B., Chandra, A., Dugad, S. R., Gupta, S. K., Jagadeesan, P., Jain, A., ... Tanaka, K. (2019, Mar). Measurement of the electrical properties of a thundercloud through muon imaging by the grapes-3 experiment. *Phys. Rev. Lett.*, *122*, 105101. Retrieved from `https://link.aps.org/doi/10.1103/PhysRevLett.122.105101` doi: 10.1103/PhysRevLett.122.105101

Heidler, F. H., Manhardt, M., & Stimper, K. (2013, April). The Slow-Varying Electric Field of Negative Upward Lightning Initiated by the Peissenberg Tower, Germany. *IEEE Transactions on Electromagnetic Compatibility*, *55*(2), 353-361. doi: 10.1109/TEMC.2012.2209121

Hurley, K., Dingus, B. L., Mukherjee, R., Sreekumar, P., Kouveliotou, C., Meegan, C., ... Niel, M. (1994, December). Detection of a γ-ray burst of very long duration and very high energy. *Nature*, *372*(6507), 652–654. Retrieved from `https://doi.org/10.1038/372652a0` doi: 10.1038/372652a0

Jackson, J. D. (1999). Classical Electrodynamics. In (3rd ed., p. 661-732). New York, United States: John Wiley & Sons, Inc. (ISBN:9780471309321) doi: 10.1002/3527600434.eap109

Kiyosi Ito and The Mathematical Society of Japan. (1993). Encyclopedic Dictionary of Mathematics. In (2nd ed., Vol. 1, p. 2168). London, England: The MIT Press. (ISBN: 0262590204)

Koch, H. W., & Motz, J. W. (1959, Oct). Bremsstrahlung cross-section formulas and related data. *Rev. Mod. Phys.*, *31*, 920–955. Retrieved from `https://link.aps.org/doi/10.1103/RevModPhys.31.920` doi: 10.1103/RevModPhys.31.920

Moss, G. D., Pasko, V. P., Liu, N., & Veronis, G. (2006). Monte Carlo model for analysis of thermal runaway electrons in streamer tips in transient luminous events and streamer zones of lightning leaders. *Journal of Geophysical Research: Space Physics*, *111*(A2), 1-37. Retrieved from `https://agupubs.onlinelibrary.wiley.com/doi/abs/10.1029/2005JA011350` doi: 10.1029/2005JA011350

–27–

Nemiroff, R. J., Norris, J. P., Kouveliotou, C., Fishman, G. J., Meegan, C. A., & Paciesas, W. S. (1994, March). Gamma-Ray Bursts Are Time-asymmetric. *Astrophysical Journal*, *423*, 432-435. doi: 10.1086/173819

Norris, J. P., Nemiroff, R. J., Bonnell, J. T., Wickramasinghe, W. A. D. T., Kouveliotou, C., Paciesas, W. S., . . . Meegan, C. A. (1994, November). Gross Spectral Differences between Bright and DIM Gamma-Ray Bursts. *Astrophysical Journal Letters*, *435*, L133. doi: 10.1086/187612

Perdrisat, C., Punjabi, V., & Vanderhaeghen, M. (2007, Oct). Nucleon electromagnetic form factors. *Progress in Particle and Nuclear Physics*, *59*(2), 694764. Retrieved from http://dx.doi.org/10.1016/j.ppnp.2007.05.001 doi: 10.1016/j.ppnp.2007.05.001

Pu, Y., Cummer, S. A., Lyu, F., Briggs, M., Mailyan, B., Stanbro, M., & Roberts, O. (2019, June). Low Frequency Radio Pulses Produced by Terrestrial Gamma-Ray Flashes. *Geophysical Research Letters*, *46*(12), 6990-6997. Retrieved from https://agupubs.onlinelibrary.wiley.com/doi/abs/10.1029/2019GL082743 doi: 10.1029/2019GL082743

Punjabi, V., & Perdrisat, C. (2014, March). The Proton Form Factor Ratio Measurements at Jefferson Lab. *EPJ Web of Conferences*, *66*, 1-4. Retrieved from https://doi.org/10.1051/epjconf/20146606019 doi: 10.1051/epjconf/20146606019

Skeltved, A. B., stgaard, N., Mezentsev, A., Lehtinen, N., & Carlson, B. (2017). Constraints to do realistic modeling of the electric field ahead of the tip of a lightning leader. *Journal of Geophysical Research: Atmospheres*, *122*(15), 8120-8134. Retrieved from https://agupubs.onlinelibrary.wiley.com/doi/abs/10.1002/2016JD026206 doi: 10.1002/2016JD026206

Whittaker, E. T., & Watson, G. N. (1927). A course in modern analysis : an introduction to the general theory of infinite processes and of analytical functions, with an account of the principal transcendental functions. In (4th ed., p. 616). The Pitt Building, Trumpington Street, Cambridge, CB2 1RP: Cambridge University Press. (ISBN: 0521091896)

Xu, W., Celestin, S., & Pasko, V. P. (2015, January). Optical emissions associated with terrestrial gamma ray flashes. *Journal of Geophysical Research: Space Physics*, *120*(2), 1355-1370. Retrieved from https://agupubs.onlinelibrary.wiley.com/doi/abs/10.1002/2014JA020425 doi: 10.1002/2014JA020425

Xu, W., Celestin, S., Pasko, V. P., & Marshall, R. A. (2019, August). Compton Scattering Effects on the Spectral and Temporal Properties of Terrestrial Gamma-Ray Flashes. *Journal of Geophysical Research: Space Physics*, *124*(8), 7220-7230. Retrieved from https://agupubs.onlinelibrary.wiley.com/doi/abs/10.1029/2019JA026941 doi: 10.1029/2019JA026941

stgaard, N., Neubert, T., Reglero, V., Ullaland, K., Yang, S., Genov, G., . . . Alnussirat, S. (2019, December). First 10 Months of TGF Observations by ASIM. *Journal of Geophysical Research: Atmospheres*, *124*(24), 14024-14036. Retrieved from https://agupubs.onlinelibrary.wiley.com/doi/abs/10.1029/2019JD031214 doi: 10.1029/2019JD031214